KeAi
CHINESE ROOTS
GLOBAL IMPACT

Available online at www.sciencedirect.com

ScienceDirect

Green Energy & Environment 6 (2021) 585–596

www.keaipublishing.com/gee

Research paper

Nanocomposite membranes with high-charge and size-screened phosphorylated nanocellulose fibrils for CO_2 separation

Ragne Marie Lilleby Helberg [a], Jonathan Ø. Torstensen [b], Zhongde Dai [a], Saravanan Janakiram [a], Gary Chinga-Carrasco [b], Øyvind W. Gregersen [a], Kristin Syverud [a,b], Liyuan Deng [a,*]

[a] *Department of Chemical Engineering, Norwegian University of Science and Technology, Trondheim, 7491, Norway*
[b] *RISE PFI, Trondheim, 7491, Norway*

Received 17 January 2020; revised 30 July 2020; accepted 16 August 2020
Available online 21 August 2020

Abstract

In this study, cellulose nanofibrils (CNF) of high charge (H-P-CNF) and screened size (H-P-CNF-S) were fabricated by increasing the charge of phosphorylated cellulose nanofibrils (P-CNFs) during the pre-treatment step of CNF production. Results show that the H-P-CNF have a significantly higher charge (3.41 mmol g^{-1}) compared with P-CNF (1.86 mmol g^{-1}). Centrifugation of H-P-CNF gave a supernatant with higher charge (5.4 mmol g^{-1}) and a reduced size (H-P-CNF-S). These tailored nanocelluloses were added to polyvinyl alcohol (PVA) solutions and the suspensions were successfully coated on porous polysulfone (PSf) supports to produce thin-film nanocomposite membranes. The humid mixed gas permeation tests show that CO_2 permeability increases for membranes with the addition of H-P-CNF-S by 52% and 160%, compared with the P-CNF/PVA membrane and neat PVA membrane, respectively.

Keywords: CO_2 separation; Nanocellulose; Phosphorylated CNF; PVA; Nanocomposite; TFC membrane

1. Introduction

The level of CO_2 in the atmosphere had increased dramatically during last decades and was reported to have passed 400 ppm in 2015 [1,2]. As consequences of this rapid increase, serious climatic change effects have been observed, including glacier melting, sea level rising, sea acidification, and extreme weather. The implementation of CCS (carbon capture and storage) has been considered one of several necessary actions to reduce the level of CO_2 emission from industrial sources [3,4]. It is well established that membrane separation is a cost-effective alternative to the traditional CO_2 separation technologies (e.g., amine absorption) thanks to their small module size, high modularity, and low negative environmental impact and energy demand [5]. Most of the commercial membranes for gas separation are polymeric membranes, where gases usually transport by the solution-diffusion mechanism [6] and are generally subjected to a trade-off between the gas permeation rate and selectivity. However, for large-scale CCS applications, such as capture of CO_2 from flue gas, both CO_2 permeance and CO_2/N_2 selectivity of the membranes must be sufficient in order to make the separation economically feasible [7].

Natural cellulose is the most abundant polymer on earth, hence nanocellulose particles have a low carbon footprint and are renewable, recyclable and non-toxic. Nanocellulose/polymer nanocomposite membranes have been demonstrated to be promising for their improved CO_2 permeance compared with the neat polymeric membranes, without sacrificing the CO_2/N_2 selectivity [8–12]. Nanocelluloses are a class of cellulose objects that have a high content of hydroxyl groups, high

* Corresponding author.
E-mail address: liyuan.deng@ntnu.no (L. Deng).

https://doi.org/10.1016/j.gee.2020.08.004

aspect ratio, high strength and a low density. Nanocellulose is usually classified as cellulose nanocrystals (CNCs), cellulose nanofibrils (CNFs) or bacterial nanocelluloses (BNCs) [13]. CNF and CNC are produced by a top-down method [14], which implies that a nanocellulose suspension contains residual fibers, larger pulp remnants, fines, nanocellulose, oligomers and monomers. Chemical pre-treatment is often a necessity in order to reduce the energy applied during production but can also be used to introduce specific properties/attributes for different applications. The classification, fabrication and application of nanocellulose has been thoroughly reviewed in the literature [15–17].

Several studies have shown that the addition of nanocellulose improves the separation performance of membranes for CO_2 capture from flue gas. Ansaloni et al. and Venturi et al. combined microfibrillated cellulose (MFC, with a surface charge of about 30 μ_{equiv} g^{-1}, average diameter of 20 nm and average length in the order of 1 μm) with Lupamin (Poly (vinylamine)) in facilitated transport membrane for CO_2 capture [8,9]. Dai et al. used commercial CNC and CNF to prepare PVA/nanocellulose membranes and demonstrated that the CO_2 separation performance of the PVA/nanocellulose TFC hollow fiber membranes was significantly improved with increasing amount of CNC [10]. Jahan et al. reported CNC/PVA and P-CNF/PVA facilitated transport membranes for biogas upgrading at feed pressures of 5–15 bar [18,19]. Very recently, Dai et al. summarized the results of nanocellulose-based hybrid membranes for CO_2 separation [20], where the need of understanding the role of nanocellulose in the transport mechanism was emphasized.

Although the interest in applying nanocellulose in membranes for CO_2 separation has increased in recent years, the effects of nanocellulose properties (such as charge and size) is not fully revealed. Our previous work was the first study that compared membranes containing different nanocellulose types [11] showing that adding commercial cellulose nanocrystals and phosphorylated CNF improved the CO_2 separation performance. This improvement is probably caused by the uniform nanoscale size of CNCs and the high charge in the P-CNF. It was hypothesized that nanocellulose could enhance CO_2 separation if it was highly charged and had nanoscale size features.

The aim of the present study is to further improve the separation performance by introducing nanocellulose with higher charge, and to investigate the effect of the nanocellulose size distribution. In this work, P-CNF with a higher charge was fabricated (H-P-CNF), and the screening of nanoscale material was achieved by centrifugation to produce H-P-CNF-S. The H-P-CNF-S sample also showed an increase in charge (3.41 mmol g^{-1} for H-P-CNF vs. 5.4 mmol g^{-1} for H-P-CNF-S). Subsequently, these tailored nanocelluloses were successfully incorporated into PVA membranes to enhance the CO_2 transport. Thin-film nanocomposite H-P-CNF-S/PVA membranes were fabricated and humid mixed gas permeation tests were performed. Experiments show that CO_2 permeability increases significantly for membranes with the addition of nanocellulose with high charge and screened size.

2. Experimental

2.1. Materials

PVA (87–89% hydrolyzed, M_w 85 000–124 000) was purchased from Sigma Aldrich (USA). De-ionized water was used as a solvent for polymer solution preparation. Cellulose nanocrystals (CNCs) were purchased from The University of Maine (manufactured at the US Forest Service's Forest Product Laboratory in Madison, Wisconsin) made by sulfuric acid hydrolysis of wood pulp and provided as an aqueous slurry of approximately 11–12 wt%.

For the preparation of phosphorylated cellulose nanofibrils, fully bleached cellulose pulp from softwood was supplied by Södra Cell (Sweden). Urea (ACS reagent) and ammonium phosphate dibasic (99%) were purchased from Sigma Aldrich (Missouri, USA). The as-received cellulose pulp was previously characterized by Torstensen et al. [21]. The flat sheet porous support is the polysulfone (PSf) ultrafiltration (UF) membrane (molecular weight cut-off (MWCO) of 50 000) purchased from Alfa Laval (Denmark). CO_2/N_2 (10 vol/90 vol) gas mixture and CH_4 (99.999%) used in gas permeation test were supplied by AGA (Norway). All chemicals used in this study were used without any purification.

2.2. Preparation and characterization of nanocellulose

2.2.1. Preparation of phosphorylated cellulose nanofibrils H-P-CNF and H-P-CNF-S

Phosphorylation was done in order to partially convert cellulose-OH to phosphate ester groups on the cellulose chains (cellulose-O-H_2PO_3) [22]. The phosphate groups may deprotonate, forming Cellulose-O-HPO_3^- or Cellulose-O-PO_3^{2-}. H-P-CNF and H-P-CNF-S were fabricated from softwood in a method similar to as reported by Torstensen et al. [11], but an extra milling step that facilitates the intrusion of chemicals [23] was introduced with the purpose of increasing the charge of the P-CNF. The starting pulp was beaten at 30 000 rounds at 21 wt% dry matter in an L&W Pulp disintegrator, and then dewatered. The beaten pulp was subsequently diluted to 10 wt % and processed in a PFI-mill with 5000 revolutions at 300 g/batch. The mass was assumed to be completely anhydrous glucose units (AGU), and 100 g of dry mass was mixed with appropriate amounts of urea (U) and diammonium hydrogen phosphate (DAHP). The mole-ratio was 1:2.5:10 (AGU:DAHP:U). The suspension was subsequently diluted to 0.5 wt % pulp and stirred in ambient conditions overnight before drying at 65 °C for 11 days. The dried pulp was divided into smaller pieces and completely dried at 65 °C (3 days), and again divided into 2–4 cm solid pieces. These were heat treated for 60 min at 150 °C in air and subsequently cooled until reaching ambient temperatures. The mass was swollen overnight in 2 L of deionized water, then rinsed to a conductance less than 4 μS cm^{-1} in a 140 mesh filter paper. The mass was then diluted to 0.8 wt% and beaten in an L&W Pulp Disintegrator at 10 000 rounds. The mass was homogenized/fibrillated with one pass at 600 bar in a Rannie 15 type

12.56X homogenizer (APV, SPX Flow Technology, Silkeborg, Denmark). The resulting mass is referred to as H-P-CNF. The mass was fractionated by ultracentrifugation (Sorval RC 5B Plus centrifuge with a SLA-1500 rotor). Centrifugation was performed on 200 g of 0.3 wt% suspension (9000 rpm for 60 min). The top 100 mL was gently removed with a pipette, and is hereafter termed H-P-CNF-S. The exact dry matter of nanocelluloses were determined by a dry-matter scale prior to application.

2.2.2. Characterization of phosphorylated cellulose nanofibrils H-P-CNF and H-P-CNF-S

The charge was determined by a conductimetric method as described elsewhere [24], with three parallels.

The nanocellulose fraction was investigated using an Atomic Force Microscopy (AFM), Dimension Icon Scanning Probe Microscope (Bruker, USA). A silicon nitride tip was employed in a ScanAsyst-Air Tapping Mode. The samples were prepared on Mica sheets by depositing a drop of diluted nanocellulose suspensions (0.005 wt%) and drying at ambient conditions for 24 h.

The macroscopic suspension morphology was analyzed with Fibertester. The presence of micron sized pulp remnants (residual fibers), including fines, was determined. Fibertester is a method to characterize the amount of residual fibers, fines and objects (including object length and width) [25,26]. These parameters are an indirect measure on how much nanocellulose is present within the nanocellulose suspension. More details about the Fibertester can be found in literature [27]. The pulp was investigated by passing two parallels of 0.1 g of dry matter through a L & W FiberTester PLUS. This step was used to extract the number of objects that have lengths between 100 μm and 10 000 μm and widths between 75 μm and 10 000 μm. Fines were defined as sample objects with lengths between 7 μm and 200 μm, thus the total amount of fines is the percentage of such particles compared to all objects that are detected by Fibertester.

The degree of fibrillation of the suspensions was also characterized by laser profilometry [26] and optical scanning [25]. These techniques are used to analyze the nanocellulose film surface morphology, which is related to the presence of micrometer-sized residual fibres in the CNF suspension.

Film optical scanning of H-P-CNF and H-P-CNF-S was performed on neat films using a Epson Perfection V750 PRO at 4800 DPI resolution [25]. Films of H-P-CNF and H-P-CNF-S were prepared by casting of equally concentrated suspensions in petri dishes before drying at room temperature.

Laser profilometry (LP) topography images were acquired using a LP (Lehmann, Lehman Mess-Systeme AG Baden-Dättwil, Germany, 10 images). H-P-CNF and H-P-CNF-S films were sputtered with a thin layer of gold (Agar Auto Sputter Coater) prior to scanning. The lateral and z-resolution of the LP system was 1 μm and 10 nm, respectively. The size of the local areas was 1 mm × 1 mm. The root-mean-square height (Sq) was quantified as a function of lateral wavelength according to Chinga-Carrasco et al. [26].

2.3. Membrane preparation and characterization

2.3.1. Solution/suspension preparation

Aqueous solutions of PVA were prepared by adding PVA to de-ionized water (4–7 wt% solutions) followed by heating under reflux (90 °C for 5 h). The desired amount of H-P-CNF/H-P-CNF-S/CNC suspensions was added to the PVA solution and the total solid content was adjusted using de-ionized water. For a better comparison of the H-P-CNF and H-P-CNF-S nanocomposite materials, all the membranes were prepared with 4% nanocellulose of the total solid content. Moreover, the effect of the H-P-CNF-S content was investigated by the preparation of H-P-CNF-S/PVA membranes (0–25 wt% H-P-CNF-S). The total concentration of solids in aqueous suspensions was 2 wt%.

The content of CNC, H-P-CNF and H-P-CNF-S (represented by $w_{nanocellulose}$, wt%) was calculated using Eq. (1).

$$w_{nanocellulose} = \frac{w_{nanocellulose}}{w_{nanocellulose} + w_{PVA}} \quad (1)$$

where $w_{nanocellulose}$ and w_{PVA} are the weight of the solid of nanocellulose and PVA, respectively.

Neat PVA as well as a membrane with 4% CNC was also prepared and tested as a reference. The PVA/nanocellulose suspensions were stirred with a magnetic stirrer for minimum 1 h followed by ultrasonication for 2 min (Fisher Scientific™ Model 505 Sonic Dismembrator, 500W, 20% power level) before membrane preparation or film preparation.

2.3.2. Nanocomposite membrane preparation

Preparation of the nanocomposite membranes was done by dip coating a flat sheet PSf UF membrane support in the respective PVA/nanocellulose suspensions. Prior to the dip coating the PSf support was washed in tap water (45–50 °C for 1.5 h) followed by washing in DI water (30 min). The support was naturally dried for approximately 30 min before masking with aluminum tape onto a glass plate to prevent the suspension from leaking into the backside of the support. The support was then dipped in the coating solution for 30 s before drying (standing vertically) for 3 h at room temperature. After drying, the second coating was performed by the same procedure, but turning the support upside-down. After drying at room temperature overnight, the nanocomposite membranes were dried in a convection oven for 3 h at 45 °C to ensure the complete removal of water, and then heat treated for 1 h at 105 °C. The selective layer is thus formed after dip coating of the PVA/nanocellulose suspensions on the flat sheet PSf UF membrane support and the subsequent evaporation of solvent.

2.3.3. Film preparation

PVA/nanocellulose films of the same compositions as the nanocomposite membranes were prepared by pouring 30–50 mL of the coating solution in PE petri dishes followed by solvent evaporation in ambient temperatures. The films were then dried and heat-treated by the same procedure as the nanocomposite membranes (3 h at 45 °C and 1 h at 105 °C)

with an additional treatment at 24 h in a vacuum oven at room temperature to ensure complete removal of any moisture in the films. The films were kept in a desiccator until the different material characterizations were performed.

2.3.4. Membrane characterization

The cross section and surface morphology of the nanocomposite membranes were evaluated by scanning electron microscopy (SEM, Hitachi TM3030 Table top). The membrane samples were freeze-fractured in liquid nitrogen to get an even cross section. All SEM samples were coated with gold for 90 s prior to evaluation, to ensure electrical conductivity (Quorum Q150 ES sputter coater).

The material properties of PVA/nanocellulose were characterized using the prepared films. Fourier-Transform Infrared Spectroscopy (FT-IR) was carried out using a Thermo Scientific Nicolet iS50 FT-IR (ATR mode). The FTIR spectrum reported is from the average of 16 scans in the wavelength range from 400 to 4000 cm^{-1}.

The thermal properties of the PVA/nanocellulose materials were evaluated by TGA (NETZSCH TG 209 Libra F1, N_2 balance gas with flow rate of 10 mL min^{-1}, N_2 sweep gas with flow rate of 60 mL min^{-1}). Each sample (~10 mg) was heated from ambient temperature to 700 °C with a heating rate of 10 °C min^{-1}. Experiments were done at least in two parallels.

The water uptake of the membrane materials was measured by a gravimetric method (humid conditions, 23 °C). Samples for testing were made by weighing PVA/nanocellulose films before placing them in a desiccator saturated with water vapor. The samples were weighed every 24 h to determine the water uptake. The percentage of water uptake was calculated using Eq. (2). The water uptake was measured for two replicates of each membrane.

$$\Omega_{water\ uptake} = \frac{W_s - W_D}{W_D} \times 100 \tag{2}$$

W_s and W_D are the weight of the swollen and dry membrane, respectively.

In this study, the gas separation performance under humid conditions was tested using a constant pressure-variable volume method in a customized mixed gas separation system (Fig. 1). Detailed information about the test rig and procedure can be found elsewhere [28]. The steady-state flux of CO_2 and N_2 in a mixed gas stream of 10% CO_2 and 90% N_2 permeating through a membrane was measured in this test. A sweep gas (CH_4) was used to provide a driving force for separation by reducing the CO_2 partial pressure on the downstream side of the membrane.

All experiments were carried out at a temperature of 25 °C with a feed pressure of 1.2 bar and a permeate side pressure of 1 bar unless otherwise specified. The relative humidity of the feed gas and the sweep gas was adjusted to 95% for all experiments by two sets of mass flow controllers unless otherwise specified. The feed flow rate (200 mL min^{-1}) and sweep flow rate (100 mL min^{-1}) was set by two Bronkhorst mass flow controllers. The process variables (pressure, temperature, gas flow rate and relative humidity of gases of feed and sweep streams) were continuously monitored and logged by the software from LabView. The total pressure is regulated by a Bronkhorst digital back-pressure regulator. The permeate stream flow rates and retentate stream flow rates were measured manually with a bubble flow meter. The concentrations of the gas streams on the upstream side and downstream side and sweep gas stream were continuously analyzed by a Micro GC Agilent 3000. The flat sheet membranes were placed in a circular stainless-steel permeation cell, with an active permeation area of 19.7 cm^2.

CO_2 permeance and CO_2/N_2 selectivity are the two most commonly used parameters to evaluate gas separation performance. The gas permeances was calculated (using a complete mixing model) from the total permeance flow, J_A, as described by Eq. (3).

$$Q_A = \frac{J_A}{x_{fA}p_f - x_{pA}p_p} \tag{3}$$

where Q_A represents the permeance of component A in the gas mixture and J_A is the flux, while x_{fA} and x_{PA} are the mole fraction of A at the feed and permeate sides, respectively. p_f and p_p are the absolute pressure in bar at the feed and permeate sides. In this study, the unit Gas Permeance Unit (GPU) is used to report the permeance for a better comparison with the literature values (1 GPU = 10^{-6} cm^3(STP) cm^{-2} s^{-1} $cmHg^{-1}$ = 2.7 × 10^{-3} m^3(STP)/m^{-2} bar^{-1} h^{-1}).

Furthermore, in order to take the thickness effect of the selective layer into account, a specifically defined term, *thickness weighed permeance* (calculated by Eq. (4)), P_t, was used in this work for the permeation property study of the selective layers containing different types and contents nanocellulose (and hence very different thicknesses), so as to conveniently compare the CO_2 permeation properties of the selective layer materials in the composite membranes. Please note that the *thickness weighed permeance* was calculated using the measured CO_2 permeances of the composite membranes and the thicknesses of their selective layers by assuming that the porous supports have negligible mass transfer resistance. Since P_t has the same unit (in Barrer) as the commonly used term "permeability" or "permeability coefficient" in the literature, for the reader's convenience, hereafter in this work "permeability" was used when we refer to the thickness weighed permeance.

$$P_t = Q \cdot l \tag{4}$$

The separation factor, $\alpha_{A,B}$, as defined in Eq. (5), was calculated and referred to as CO_2/N_2 selectivity throughout the report.

$$\alpha_{A,B} = \frac{y_A^d}{y_B^d} \Big/ \frac{y_A^u}{y_B^u} \tag{5}$$

where y_A^d and y_B^d are the molar fractions of A and B at the downstream (permeate) side and y_A^u and y_A^u are the molar fractions of A and B at the upstream (feed) side, respectively.

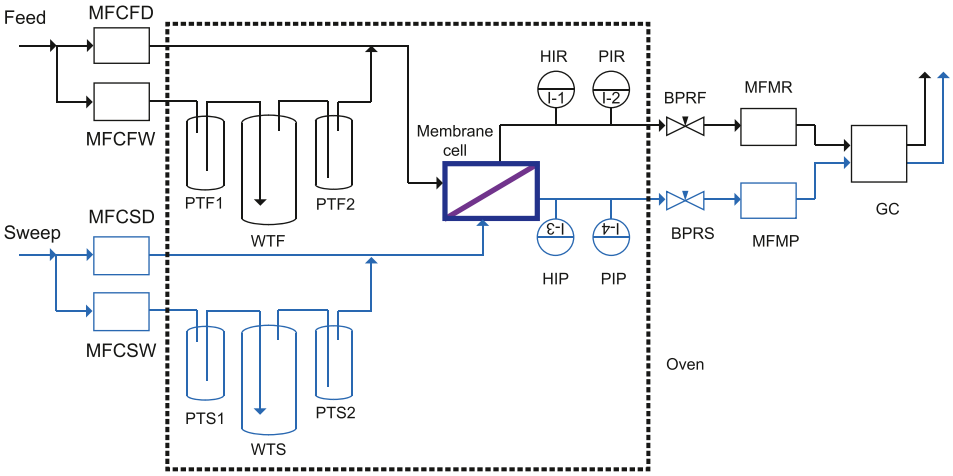

Fig. 1. Mixed gas permeation set up. MFCFD (mass flow controller for feed side, dry gas); MFCFW (mass flow controller for feed side, wet gas); WTF (water tank, feed side); PTF1 and PTF2 (protective tanks, feed side); HIR and PIR (Humidity and pressure indicator, retentate side); BPRF (back pressure regulator, feed side); MFMR (mass flow meter, retentate side); MFCSD (mass flow controller dry gas, sweep side); MFCSW (mass flow controller wet gas, sweep side). WTS (water tank, sweep side); PTS1 and PTS2 (protective tanks, sweep side); HIP and PIP (humidity and pressure indicator, permeate side); BPRS (back pressure regulator, sweep side); MFMP (mass flow meter, permeate side); GC (gas chromatograph). Reproduced with permission from [29].

The gas permeation parameters are calculated by an average of minimum of 2 h measurement after steady-state is reached. A minimum of two membranes are tested each time and the reported errors are standard deviation of the representative measurements.

3. Results and discussion

3.1. Nanocellulose characterization

The major results from the nanocellulose characterization are presented in Table 1. The characterization results of P-CNF from our previous work [11] are included as a reference.

The H-P-CNF charge was determined to be 3.41 ± 0.09 mmol g^{-1}, which is considerably higher than the literature value [22]. The increase is explained by the additional PFI milling step (a technique which is known to swell the pulp and facilitate the intrusion of chemicals) [23] and to the pre-cutting of samples into small pieces (2–4 cm) prior to the final heat treatment. The effect of these steps was observed by a reduction in the required homogenization; a reduction from two homogenization passes in previous study (at 1000 bar and 600 bar respectively) to one homogenization passes in this study (at 600 bar), correspondingly to significant energy saving (about 1000 kWh ton^{-1}). The H-P-CNF-S charge was 5.4 ± 0.2 mmol g^{-1}, likely due to the smaller fibrils and hence a bigger available surface area contained within this fraction.

Table 1
Nanocellulose characterization results.

	H-P-CNF	H-P-CNF-S	P-CNF [11]
Charge (mmol g^{-1})	3.41 ± 0.09	5.4 ± 0.2	1.86 ± 0.012
Nanocellulose width (nm)	3.4 ± 0.9	1.9 ± 0.9	2.85 ± 0.6
Total amount of fines (%)	81 ± 0	98 ± 0	50.2 ± 1.7
Secondary fines (%)	54.7 ± 0.2	89.4 ± 0.1	29.3 ± 0.2

The nanocellulosic fraction was investigated by AFM and the widths of the fibrils were extracted from the AFM imaging, as reported in our prior work by Torstensen et al. [11]. Fig. 2 gives the overview images of H-P-CNF and H-P-CNF-S, showing evident difference in the fiber lengths and widths.

Based on our prior work, the fraction of fines and secondary fines should be high for the given nanocellulose to improve its effect on gas separation performance, which was the case for both the new H-P-CNF and H-P-CNF-S applied in this study.

The P-CNF used in this work contained approximately 50% fines. Conversely, the H-P-CNF contained ~80% fines. This may be explained by the enhanced milling during fabrication and the higher charge in this batch. Secondary fines is a marker of material fibrillation to nanocellulose [27] and the concentration of secondary fines were increased significantly in this study (~54%) as compared to the original P-CNF (~29%) [11]. The content of fines in H-P-CNF-S increased to 98% with 89.4% secondary fines, showing significant size screening effect by centrifugation. Also, H-P-CNF-S had the shortest fines.

An indirect measurement of fibrillation may also be realized by investigating the micrometer features of produced films as characterized by optical analysis (Fig. 3a and b). These elongated objects observed in Fig. 3b are micrometer sized residual fibers. The optical analysis images show that there are more visible residual fibers for the H-P-CNF film compared to the H-P-CNF-S film. The light transmittance through films cast from H-P-CNF-S was higher and more homogeneous compared to H-P-CNF, which evidenced larger fraction of residual fibers shown by the arrows in Fig. 3b. Laser profilometry were performed to further quantify the roughness of films which is an indication of the degree of fibrillation [26]. The images from laser profilometry (Fig. 3c and d) clearly demonstrate the decreased roughness in H-P-CNF-S compared to H-P-CNF films. The roughness as detected with laser profilometry was quantified by analyzing

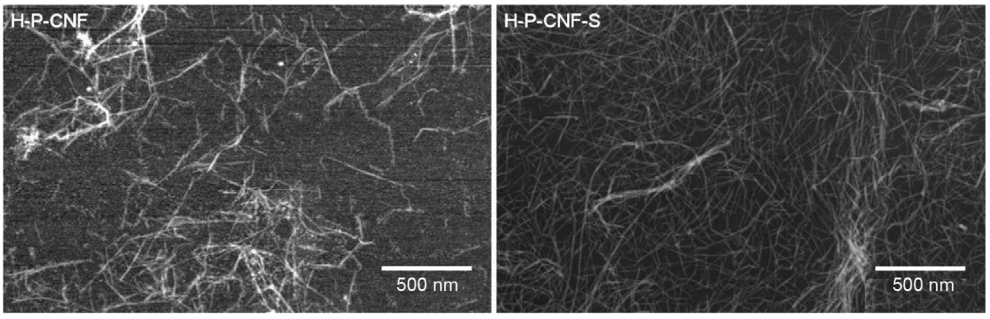

Fig. 2. AFM micrographs of H-P-CNF and H-P-CNF-S.

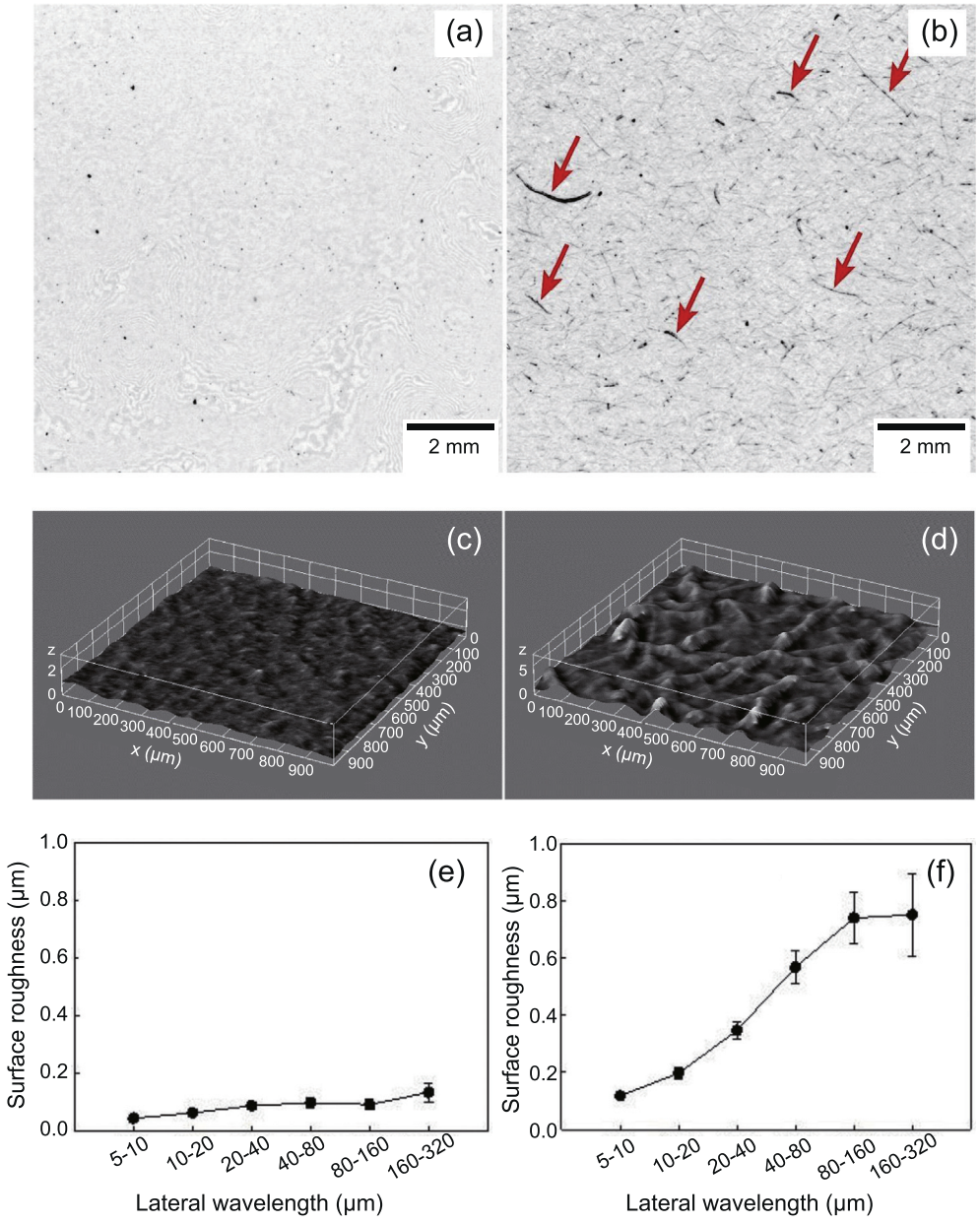

Fig. 3. Optical images of sample films containing H-P-CNF-S (a) and H-P-CNF (b). The red arrows indicate residual fibers. Roughness maps (1 × 1 mm) of H-P-CNF-S films (c) and H-P-CNF films (d). Surface roughness of films as a function of lateral wavelength of H-P-CNF-S (e) and H- P-CNF (f).

profiles using a FFT (Fast Fourier Transform) filter. The root-mean square roughness could thus be expressed as a function of lateral wavelength, which may be regarded as the size of the feature (e.g. cellulose fiber) that creates the roughness and is plotted in Fig. 3e and f.

3.2. Membrane characteristics

3.2.1. Membrane morphology

SEM imaging was carried out to evaluate the morphology and selective layer thickness of the membranes. Even and homogeneous surfaces were obtained without defects for all the membranes. The cross-section and surface images for the H-P-CNF-S/PVA nanocomposite membrane are presented in Fig. 4. SEM images of H-P-CNF/PVA membranes, CNC/PVA membranes and neat PVA membranes are very similar except for the different thicknesses, thus are not presented. The selective layer thicknesses of all the membranes measured by SEM are given Table 2. The membranes were prepared by the same coating method and with the same suspension contents. However, the selective layer thicknesses were varying due to the difference of the suspension viscosities. Moreover, it is evident that the different nanocelluloses have a slightly different effect on the selective layer thickness even with similar viscosity; The selective layer thickness is higher for the H-P-CNF/PVA membrane (1025 nm) than H-P-CNF-S/PVA membrane (820 nm) while the thickness of the CNC/PVA membrane is more similar (662 nm) to the neat PVA membrane (493 nm). Dai et al. also observed that the addition of CNC has a less effect on the selective layer thickness compared with CNF [10]. The different shape, strength, and surface properties of the nanocellulose fibers also contribute to the differences in thicknesses of the coating layers.

3.2.2. FTIR analysis

Fig. 5a shows the FT-IR spectra of the neat H-P-CNF, neat H-P-CNF-S and neat PVA, while Fig. 5b) shows the FT-IR spectra of the respective nanocomposites. The broad peak at 3000 cm^{-1} to 3500 cm^{-1} represents the O-H vibrations. Although all samples were dried before the tests, some samples might have still absorbed water from the surroundings, which could affect the peak intensity. Fig. 5a shows that the spectra of H-P-CNF and H-P-CNF-S are identical. The bands at 1239 cm^{-1}, 1022-1027 cm^{-1} and 907-944 cm^{-1} are the peaks attributed to the phosphorylation [22,30]. The other

Table 2
Selective layer thicknesses of the different membranes.

	Selective layer thickness (nm)	St.dev (nm)
H-P-CNF/PVA	1025	309
H-P-CNF-S/PVA	820	122
CNC/PVA	662	51
PVA	493	142

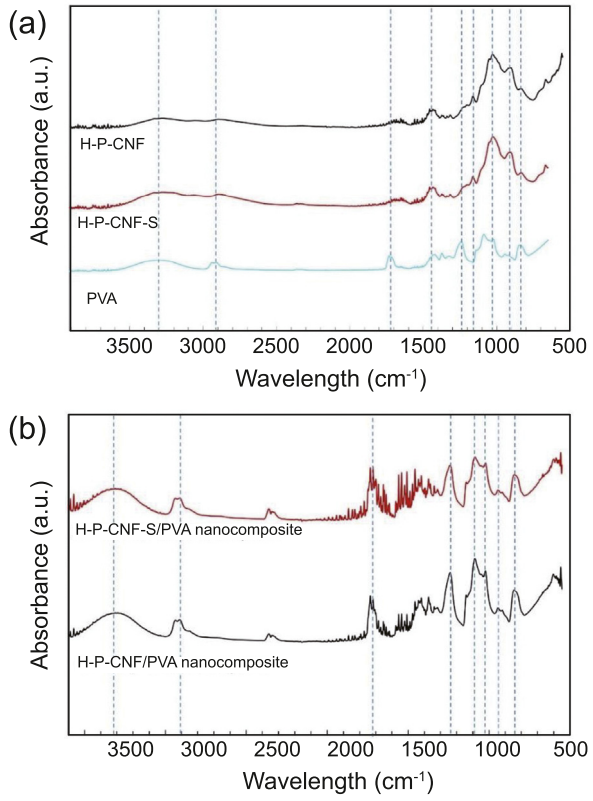

Fig. 5. FT-IR spectra of (a) neat H-P-CNF, neat H-P-CNF-S and neat PVA, (b) H-P-CNF/PVA nanocomposite and H-P-CNF-S/PVA nanocomposite.

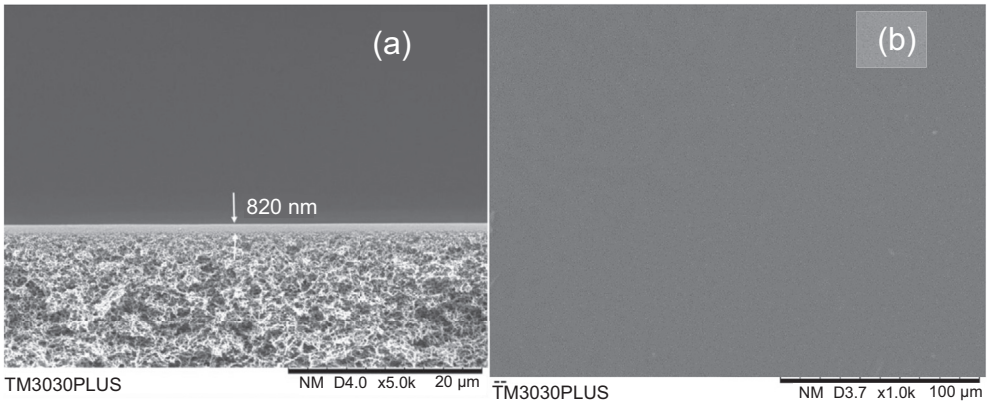

Fig. 4. (a) Cross sectional morphology of H-P-CNF-S/PVA nanocomposite membranes coated on PSf support and (b) Surface morphology of H-P-CNF-S/PVA.

peaks specific for neat P-CNF's and PVA are shown in the given detailed peak assignment report in Table 3. The spectra for the nanocomposites are shown in Fig. 5b, where PVA peaks are the dominating ones as PVA is main component of the nanocomposites.

3.2.3. Thermal properties

TGA analysis was carried out to investigate the thermal stability of neat H-P-CNF and H-P-CNF-S, as presented in Fig. 6a. CNC and PVA were used as references. The thermal stability of the respective nanocomposites was also investigated and results are presented in Fig. 6b. As it can been seen from Fig. 6a, both neat H-P-CNF and neat H-P-CNF-S has a similar T_{onset} (200 °C and 195 °C respectively). The results obtained are in accordance with the findings of Ghandapour et al. [22], which obtained a T_{onset} at 258 °C for P-CNF. Ghandapour reports TGA curves for nanosheets/nanofilms prepared with lower reaction times of phosphorylation of fibers which might explain the difference in T_{onset}. The obtained T_{onset} of H-P-CNF and H-P-CNF-S are slightly lower than for CNC (255 °C) and PVA (295 °C). Ghandapour et al. observe a similar effect of decreasing T_{onset} when introducing phosphorous to CNF. The results from the TGA characterization of the neat nanocelluloses (6a) also shows that residue content of H-P-CNF and H-P-CNF-S is higher compared to both CNC and PVA. At 700 °C, as much as 50% of the samples is still not decomposed. Similar results are obtained by Ghandapour where they apply P-CNF as a flame-retardant material, although a slightly lower final residual is obtained in their study (40%). Dai et al. obtained a T_{onset} of 280 °C for PVA as well as CNC/PVA nanocomposite materials.

As Fig. 6b shows, the PVA/nanocellulose nanocomposites have the same T_{onset} as PVA, indicating that PVA is the dominating phase. H-P-CNF-S shows a slightly different decomposition curve, but this is not considered as an important/significant deviation. The results from TGA characterization show that the thermal stability of both H-P-CNF and P-CNF-S and their respective nanocomposites is sufficient for the application in post-combustion CO_2 capture from power plant flue gas [7].

Table 3
FT-IR peak assignments [22,29,30].

Wavenumber (cm^{-1})	Peak assignment
3275–3308	O-H stretching
2912	$(C\text{-}H)_n$ strecthing
1710–1720	C=O stretching of ketone[a]
1653–1681	C=O stretching of lactam (amide II band)
1456	CH_2 bending
1239	C-O stretching ether linkage (PVA)
1150	P=O asymmetric stretching
1022–1087	C-O stretching primary alcohol, P-O-C vibration, O-P vibration
907–944	P-O-H vibrational modes
823–846	O-H out of plane bending

[a] PVA used in this study has a hydrolysis degree of 87–89%, hence about 11–13% acetate groups are present in the polymer structure.

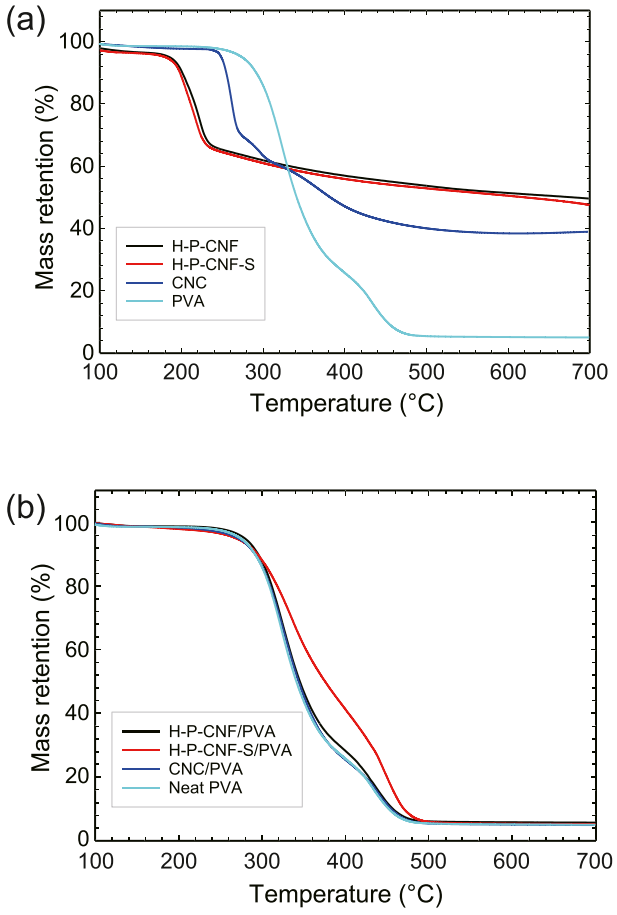

Fig. 6. TGA of neat nanocellulose films (a) and nanocomposites with PVA as the matrix polymer (b).

3.2.4. Water uptake

Fig. 7 shows the water uptake of the H-P-CNF and H-P-CNF-S and their respective nanocomposites. PVA and CNC/PVA nanocomposite were used as references. As it can be seen in Fig. 7a, both H-P-CNF/PVA and H-P-CNF-S/PVA nanocomposites have a relatively high water uptake similar to that of neat PVA, which is an advantageous feature for applications involving CO_2 separation from flue gas with presence of water vapor.

The effects of H-P-CNF-S content were studied with commercial CNC as a reference, as shown in Fig. 7b. The water uptake is presented as a function of increasing content of H-P-CNF-S from 0 to 25%. The nanocomposite with 5% H-P-CNF-S showed a lower water uptake (56%) than neat PVA (59%), which is in accordance with results in Fig. 7a. However, the addition of 10 and 25% H-P-CNF-S slightly increased the water uptake compared to neat PVA, as indicated in the figure. The lower water uptake of the 5% H-P-CNF-S nanocomposite compared to neat PVA may be attributed to the reinforcement effect of nanocellulose fiber, while the observed increase in the water uptake for the higher H-P-CNF-S content of 10% and 25% nanocomposites is most likely due to the higher charge on the surface of H-P-CNF-S nanofibers. At the

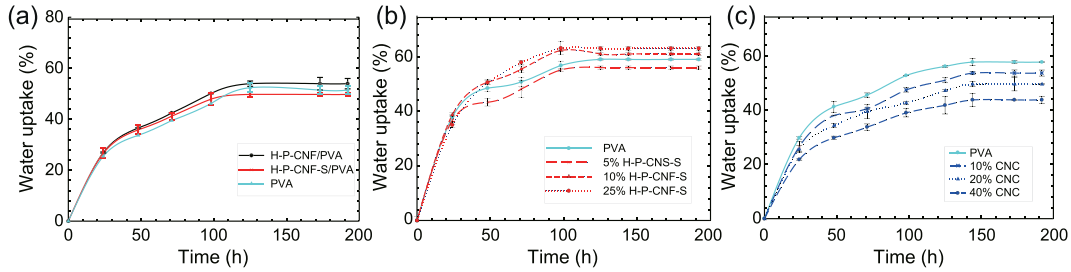

Fig. 7. Water uptake as function of time of (a) the 4 wt% H-P-CNF and H-PCNF-S in PVA and neat PVA, (b) H-P-CNF-S/PVA nanocomposites (0–25% H-P-CNF-S in PVA), (c) CNC/PVA nanocomposites (0–40% CNC in PVA).

lower content of nanocellulose addition, the reinforcement effect is believed to dominate, but at higher levels the charge effect takes over; After the charge and the reinforcement effects of nanocellulose reach a balance, further increase of nanocellulose will increase the water uptake of the nanocomposites.

On contrary to the H-P-CNF-S/PVA samples, as shown in Fig. 7c, the water uptake of CNC/PVA nanocomposites decreases monotonously with the increasing CNC content. Compared to CNC, the more hydrophilic surface of H-P-CNF-S due to the high charge may benefit the water uptake and is advantageous for CO_2 transport. As compared to neat PVA, it is expected that the nanocomposites have the potential of forming hydrophilic or water-rich channels for CO_2 transport along the nanocellulose/PVA interphases. Water is expected to be redistributed along the PVA/nanocellulose interface due to the nanocellulose charges and high hydrophilicity as compared to the neat PVA.

3.3. Membrane permeation properties

The mixed gas permeation tests using humid CO_2/N_2 (10%/90% vol) as feed gas were performed at 1.2 bar and 25 °C to evaluate the CO_2 separation performance of the modified nanocellulose-based membranes and to study the effects of the increased charge (H-P-CNF) and screened size (H-P-CNF-S) in the nanocellulose.

3.3.1. Effect of H-P-CNF and H-P-CNF-S addition

The separation performances of the membranes containing H-P-CNF and H-P-CNF-S are presented in Fig. 8. The results of neat PVA membrane and the nanocellulose/PVA membranes containing P-CNF and commercial CNC are also given as references. All the nanocellulose-based membranes contain 4 wt% nanocellulose in PVA. As it can be seen, the H-P-CNF/PVA membrane has a significantly higher CO_2 permeability compared to the P-CNF/PVA and neat PVA membranes, by 35% and 130%, respectively. The CO_2/N_2 selectivity also increases to 51, which is an around 42% increment compared to the neat PVA membrane and a ~20% increment compared to the P-CNF/PVA membrane. The notable increase in CO_2 permeability is believed attributed to the significant increase in the charge on the nanocellulose surface. From Fig. 8 it also can be seen that the size screened nanocellulose H-P-CNF-S gives the best separation performance, the CO_2 permeability of which is 160% higher than that of the neat PVA membrane and 52% higher compared to that of the P-CNF/PVA membrane, showing the positive effect of size screening of the nanocellulose by centrifugation. Moreover, it is found that the addition of H-P-CNF-S also exhibited significantly higher CO_2 permeability compared with the CNC/PVA membrane (~30% increment), implying that the charges play an important role in CO_2 transport through the membranes. It is worth noting that the increase in selectivity seems less significant, which is reasonable as the N_2 permeation is also enhanced to a certain extent by the addition of nanocellulose.

3.3.2. Effect of the H-P-CNF-S content

The effect of the H-P-CNF-S content on separation performance was also investigated, as presented in Fig. 9. To achieve proper centrifugation, the H-P-CNF suspension had to be diluted to 0.3 wt%, and the extracted supernatant (H-P-CNF-S) had a solid content of ~0.1 wt%, hence the total solids of the membranes were decreased from 2 wt% to 0.5 wt% in order to increase the attainable level of H-P-CNF-S samples. Thus, the maximum achievable content of H-P-CNF-S in the membrane was 25%. The results from the content effect study show that the CO_2 permeability is ~3.5 times higher for the 10% H-P-CNF-S/PVA membrane than the neat PVA

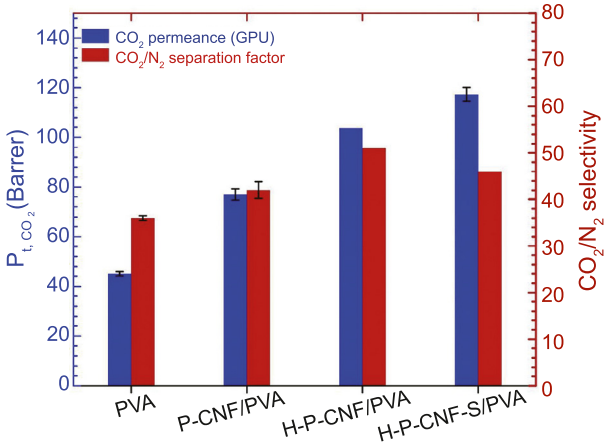

Fig. 8. Effect of H-P-CNF and H-P-CNF-S on separation performance. Tested at RT and feed pressure of 1.2 bar using CO_2/N_2 mixed gas at maximum relative humidity.

membrane. However, by increasing the H-P-CNF-S content to 25 wt%, the CO_2 permeability of the membrane decreases significantly, while the CO_2/N_2 selectivity increased marginally from 28 to 38 with the content of H-P-CNF-S increasing from 0% to 25%. The notably reduced CO_2 permeation property of the membrane containing 25 wt% can be attributed to the barrier properties of the larger amount of nanocellulose introduced to the membrane.

The optimum content of H-P-CNF-S is 10 wt%; thus, the membrane containing 10% H-P-CNF-S was selected for further investigation to study the effect of relative humidity on separation performance. It should be noted that the gas permeation tests related to the H-P-CNF-S content optimization were performed using feed pressure of 2 bars instead of 1.2 bar in order to maximize the driving force across the membrane, which gives a more significant difference between membrane performances for a better comparison.

3.3.3. Effect of relative humidity

As CO_2 separation from flue gases is the target application in this study, it is of great interest to study the effect of increasing relative humidity on the membrane separation performance. Fig. 10 shows the result of the gas permeation testing at different relative humidity. For a better comparison with the literature, here the permeation property is reported as the CO_2 permeance in GPU.

As Fig. 10 shows, at 50% RH and below, both the CO_2 permeance and N_2 permeance was close to 0. At RH below 50%, the nanocellulose fibers are densely packed and usually function as gas barriers like in most packaging coatings, which hinder the transport of gas molecules through the membranes. By increasing the relative humidity to 75%, however, the nanocellulose membranes become more permeable, especially for CO_2; thus, the CO_2/N_2 selectivity increases significantly (from ~3 to 21) even though with only a slight increase in CO_2 permeance, since N_2 permeance has not much increased. In this RH range, the increase in CO_2 permeance may be attributed to the slight increase in the distance between nanocellulose fibers and the polymer phase due to the increasing water swelling at higher RH. The polar and smaller CO_2 molecule (kinetic diameter 0.34 nm) can transport but N_2 (kinetic diameter 0.36 nm) will still be retained by the membrane, leading to a molecular sieving effect. The results show that CO_2 permeance is generally low in the RH range below 90%, but it increases with the increasing RH and follows nearly an exponential increase in the RH range from 90% RH to the fully humidified conditions. However, the increase in RH from 80% does not have a much impact on the CO_2/N_2 selectivity. In this high RH range, the permeability of both CO_2 and N_2 increased due to the swelling and the consequent loss of sieving effect due to the larger space between the nanocellulose fibers and polymer. Other studies have also reported similar effect of the relative humidity on the nanocellulose membrane separation performance [10,11,20].

3.3.4. CO_2 transport through the membrane

In this study, it is found that both H-P-CNF/PVA and H-P-CNF-S/PVA nanocomposite membranes have significant higher CO_2 permeability than the neat PVA membrane. The obtained results suggest that higher charge and small size are critical properties in nanocellulose membranes for CO_2 separation with the presence of water vapor. The nanocellulose charge induces the redistribution of water throughout the nanocomposite membrane selective layer along the PVA/nanocellulose interphase, where the more highly charged surface will attract more water. The size screened H-P-CNF-S disperses better in the PVA matrix and have a larger surface area per volume. In the water-rich regions at the PVA/nanocellulose interfaces, more CO_2 may be dissolved. Also, a charged nanocellulose surface is more CO_2-philic and will by itself attract CO_2. The addition of H-P-CNF-S in membranes has resulted in a higher CO_2 permeability than that of commercial CNCs. However, based on the findings from our previous study [11], CNC's uniform size and high fraction of nanoscale constituents were the properties that ascribed to giving the highest separation performance of the nanocomposite membranes, including the P-CNF/PVA membranes. Since H-P-CNF-S have more and larger pulp remnants

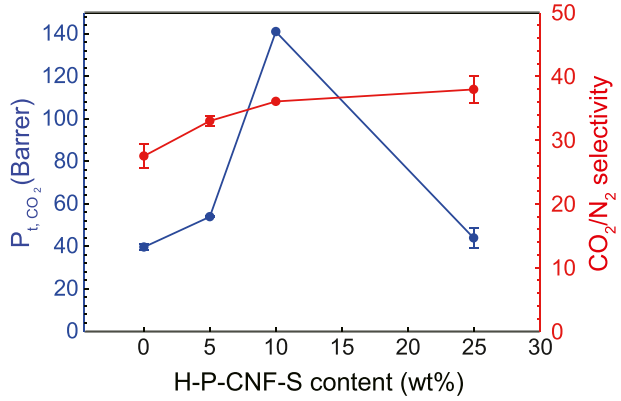

Fig. 9. The effect of the H-P-CNF-S content on separation performance. Tested at RT and feed pressure of 2.0 bars using fully humidified CO_2/N_2 mixed gas.

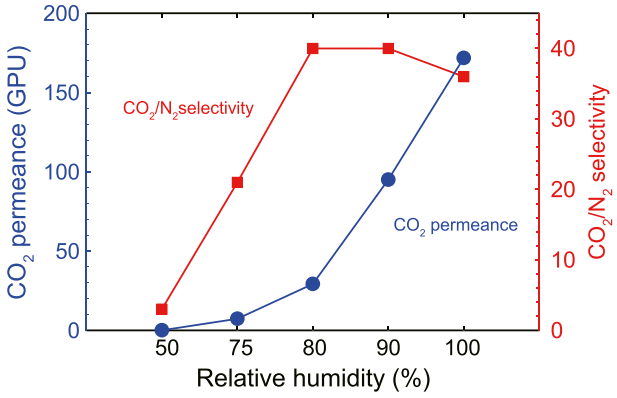

Fig. 10. The effect of relative humidity on separation performance of H-P-CNF-S/PVA nanocomposite membranes. The tested membrane is 10% H-P-CNF-S in PVA. Tested at RT and feed pressure of 2 bar using CO_2/N_2 mixed gas.

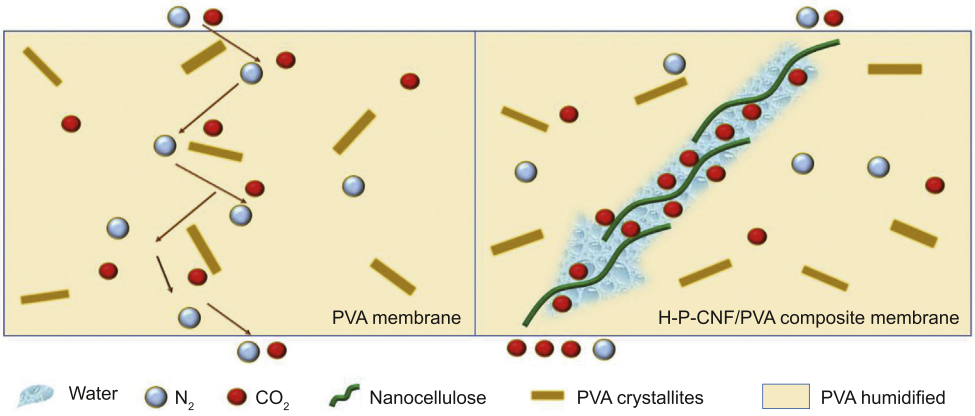

Fig. 11. CO_2 Transport in nanocellulose-based nanocomposite membranes.

compared to CNC, the high charge is reasonable to be the dominating property for the higher CO_2 permeance. Moreover, for H-P-CNF-S/PVA nanocomposite of 10% and 25%, the water uptake is slightly higher compared with the neat PVA, but for CNC/PVA nanocomposite, water uptake monotonically decreases with the increasing CNC contents, suggesting that H-P-CNF-S attracts more water than CNC to the PVA/nanocellulose interface, and it is most likely due to its highly charged nature. Based on the water uptakes of the membranes containing various types and amounts of nanocellulose and their corresponding permeation results, a hypothesized mechanism on the enhancement of CO_2 transport in this type of nanocellulose-based membranes is speculated, as shown in Fig. 11. Adding H-P-CNF-S increases the water content, which contributes to an increase in the gas permeation due to a looser matrix. Moreover, water also to an extent increases CO_2 transport by the formation of HCO_3^-.

4. Conclusions

In this study, nanocelluloses with high charge (H-P-CNF) and high charge with screened size (H-P-CNF-S) were prepared and integrated to a PVA matrix. The improved separation performance at high relative humidity conditions makes the H-P-CNF-S/PVA nanocomposite membranes a promising material for CO_2 separation at humidified conditions. Nanocomposite membranes with significantly higher CO_2 permeability (117 Barrer) than the similar membranes containing P-CNF (77 Barrer) were obtained. The CO_2/N_2 selectivity of the membrane slightly increased as well. Compared to neat PVA, the H-P-CNF-S/PVA nanocomposite membranes had a 160% increase in the CO_2 permeability.

This study confirms the hypothesis that high charge and small size are beneficial nanocellulose properties when used in nanocomposite membranes for CO_2 separation under humid conditions. The fact that the new H-P-CNF-S gives significantly better CO_2 permeability than the uniform and small sized commercial CNC implies that charge in nanocellulose is a critical property. The nanocellulose charge induces the redistribution of water throughout the nanocomposite membrane selective layer along the PVA/nanocellulose interphase, forming the water-rich region, where more CO_2 may be dissolved. Moreover, the highly charged nanocellulose surface is more CO_2-philic and will also by itself attract more CO_2.

Conflict of interest

The authors declare that there is no conflict of interest regarding the publication of this article.

Acknowledgements

The authors want to thank the Research Council of Norway for the financial support to the work through the Nano 2021 program (NanoMBE project, number 239172). We thank Södra Cell for supplying the cellulose pulp and Ingebjørg Leirset, Johnny Kvakland Melbø and Anne Reitan for support in the lab.

References

[1] J. Hansen, M. Sato, P. Hearty, R. Ruedy, M. Kelley, V. Masson-Delmotte, G. Russell, G. Tselioudis, J. Cao, E. Rignot, I. Velicogna, B. Tormey, B. Donovan, E. Kandiano, K. Von schuckmann, P. Kharecha, A.N. Legrande, M. Bauer, K.W. Lo, Atmos. Chem. Phys. 16 (2016) 3761–3812.
[2] M. Tong, Y. Lan, Q. Yang, C. Zhong, Green Energy Environ. 3 (2018) 107–119.
[3] R.K. Pachauri, M. Allen, V. Barros, J. Broome, W. Cramer, R. Christ, J. Church, L. Clarke, Q. Dahe, P. Dasgupta, Climate Change 2014: Synthesis Report, IPCC, Geneva, Switzerland, 2014, pp. 151–165.
[4] H.K. Knuutila, R. Rennemo, A.F. Ciftja, Green Energy Environ. 4 (2019) 439–452.
[5] R.W. Baker, B.T. Low, Macromolecules 47 (2014) 6999–7013.
[6] P. Bernardo, E. Drioli, G. Golemme, Ind. Eng. Chem. Res. 48 (2009) 4638–4663.
[7] T.C. Merkel, H. Lin, X. Wei, R. Baker, J. Membr. Sci. 359 (2010) 126–139.
[8] L. Ansaloni, J. Salas-Gay, S. Ligi, M.G. Baschetti, J. Membr. Sci. 522 (2017) 216–225.
[9] D. Venturi, D. Grupkovic, L. Sisti, M.G. Baschetti, J. Membr. Sci. 548 (2018) 263–274.

[10] Z. Dai, J. Deng, Q. Yu, R.M.L. Helberg, S. Janakiram, L. Ansaloni, L. Deng, ACS Appl. Mater. Interfaces 11 (2019) 10874–10882.
[11] J.Ø. Torstensen, R.M.L. Helberg, L. Deng, Ø.W. Gregersen, K. Syverud, Int. J. Greenhouse Gas Control 81 (2019) 93–102.
[12] S. Janakiram, X. Yu, L. Ansaloni, Z. Dai, L. Deng, ACS Appl. Mater. Interfaces 11 (2019) 33302–33313.
[13] A. Dufresne, Curr. Opin. Colloid Interface Sci. 29 (2017) 1–8.
[14] C. Liu, H. Du, L. Dong, X. Wang, Y. Zhang, G. Yu, B. Li, X. Mu, H. Peng, H. Liu, Ind. Eng. Chem. Res. 56 (2017) 8264–8273.
[15] A. Dufresne, Nanocellulose: From Nature to High Performance Tailored Materials, De Gruyter, Berlin, 2012.
[16] R.J. Moon, A. Martini, J. Nairn, J. Simonsen, J. Youngblood, Chem. Soc. Rev. 40 (2011) 3941–3994.
[17] D. Klemm, F. Kramer, S. Moritz, T. Lindström, M. Ankerfors, D. Gray, A. Dorris, Angew. Chem. Int. 50 (2011) 5438–5466.
[18] Z. Jahan, M.B.K. Niazi, M.-B. Hägg, Ø.W. Gregersen, J. Membr. Sci. 554 (2018) 275–281.
[19] Z. Jahan, M.B.K. Niazi, M.-B. Hagg, Ø.W. Gregersen, A. Hussain, Separ. Sci. Technol. (2019) 1–11.
[20] Z. Dai, V. Ottesen, J. Deng, R.M.L. Helberg, L. Deng, Fibers 7 (2019) 40.
[21] J.Ø. Torstensen, M. Liu, S.-A. Jin, L. Deng, A.I. Hawari, K. Syverud, R.J. Spontak, Ø.W. Gregersen, Biomacromolecules 19 (2018) 1016–1025.
[22] M. Ghanadpour, F. Carosio, P.T. Larsson, L. Wågberg, Biomacromolecules 16 (2015) 3399–3410.
[23] M. Henriksson, G. Henriksson, L.A. Berglund, T. Lindström, Eur. Polym. J. 43 (2007) 3434–3441.
[24] T. Saito, A. Isogai, Biomacromolecules 5 (2004) 1983–1989.
[25] G. Chinga-Carrasco, Micron 48 (2013) 42–48.
[26] G. Chinga-Carrasco, N. Averianova, O. Kondalenko, M. Garaeva, V. Petrov, B. Leinsvang, T. Karlsen, Micron 56 (2014) 80–84.
[27] J. Colson, W. Bauer, M. Mayr, W. Fischer, W. Gindl-Altmutter, Cellulose 23 (2016) 2439–2448.
[28] R.M. Lilleby Helberg, Z. Dai, L. Ansaloni, L. Deng, Green Energy Environ. 5 (2020) 59–68.
[29] Z. Dai, L. Ansaloni, D.L. Gin, R.D. Noble, L. Deng, J. Membr. Sci. 523 (2017) 551–560.
[30] Z.H. Ping, Q.T. Nguyen, J. Néel, Makromol. Chem. 190 (1989) 437–448.